



ADVANCED MODEL DEVELOPMENT FOR JOINTED PRECAST CONCRETE CONNECTIONS UTILISING UNBONDED POST-TENSIONED PRESTRESS

G. W. Rodgers¹, J. B. Mander² and J. G. Chase³

ABSTRACT

Damage-free structural design methods have received significant research attention in recent years due to large costs associated with sacrificial design methods. In particular, jointed precast concrete connections with unbonded, post-tensioned prestress have been the focus of a significant amount of this research. These systems provide damage-free inelastic response through gap-opening at the beam-column interface instead of through yielding and damage of the structural elements. A model that captures all the different connection characteristics and provides an accurate prediction of connection response is a useful tool for performance based analysis and design. A time-incremental model of the connection behavior is developed that accounts for yielding of the prestressing tendons, reduction or elimination of the prestressing force, friction between the post-tensioning tendons and the containing ducts, and asymmetry from non-centrally located tendons. The model is formulated using incremental versions of smooth functions to provide a continuous loading and unloading representation of behavior. The model is validated against experimental results for full-scale jointed precast concrete connection subassemblage tested with reversed sinusoidal inputs up to 4% drift. Results show very good agreement between the model and experimental results, with errors generally well less than $\pm 5\%$.

Introduction

Cast insitu reinforced concrete or monolithic precast concrete structures resist earthquake ground motions by dissipating energy in plastic hinge zones located at beam ends adjacent to the beam-column joint. But seismic response can lead to significant damage and degradation at such beam-column connections. The development of precast concrete systems with unbonded post-tensioned prestressed jointed connections that provide dissipative non-linear response due to gap-opening, instead of through structural damage in a plastic hinge zone, has been the focus of recent research (Priestley et al. 1999; Li et al. 2008; Solberg 2007). Such connections utilising Damage Avoidance Design (DAD) principles (Mander 2004) typically have low inherent damping.

Structural response for a jointed precast system is a combination of elastic member deflection and rigid body rotation. This study investigates the independent effects of elastic sub-assembly deformation and post-gap opening rigid-body rotation of the structural elements. Previous research has developed simple yet effective models for this type of jointed precast connection which provide good agreement with experimental results (Li et al. 2008).

¹ Postdoctoral Researcher, Dept. of Mechanical Engineering, University of Canterbury, Christchurch, New Zealand

² Inaugural Zachry Professor, Zachry Dept. of Civil Engineering, Texas A&M Univ., College Station, TX, USA

³ Professor, Dept. of Mechanical Engineering, University of Canterbury, Christchurch 8140, New Zealand

Although the previous research of Li et al.(2008) provided a simple explicit model describing the overall pushover behaviour, their model does not include several aspects of connection performance. While the model incorporates yielding of the tendons, it does not incorporate the prestress force reduction on subsequent cycles. The previous model provides upper and lower bounds to represent the force contributions due to friction. However, the unloading is based on a signum function and acts as a simple switch which does not capture the initial unloading stiffness due to tendon relaxation. The previous model will likely provide accurate results for jointed precast prestressed connections that utilise straight tendon profiles, and have low inherent friction, if no tendon yield is observed. However, if any notable friction is present or if tendon yield occurs, the model will not provide accurate results. Therefore, the modeling presented herein extends this earlier work to incorporate friction in the prestressing system, and changes to subsequent cycles from tendon yield. The model moves to a time-incremental form with different loading and unloading stiffness to capture friction and yielding.

Experimental Investigation

The model proposed herein is validated against experimental results using a full-scale beam-column subassembly. The 3D subassembly represents an interior joint of a ten-storey reinforced concrete building (Rodgers et al. 2008). The subassembly consisted of a seismic beam cut at its midpoint and an orthogonal gravity beam. All beams were 560mm deep and 400mm wide, framing into a 700mm square column. The orthogonal beam is referred to as the gravity beam, and was designed for one-way precast flooring panels. The other beam is referred to as the seismic beam, designed predominantly for seismic forces. This study investigates the contributions of unbounded post-tensioned prestress to seismic response based on uni-directional testing of the seismic beams. The beam prestress system consisted of two concentric 26.5mm diameter unbonded and post-tensioned prestressing thread-bars. Photographs, diagrams, and design details can be found elsewhere in Solberg (2007) and Rodgers (2009).

Modeling Connection Behavior

Overall joint hysteresis for un-bonded post-tensioned prestressed concrete DAD connections is a combination of elastic member deflection and rigid body rotation. The presence of the un-bonded post-tensioned prestress initially delays gap opening. Lateral column deflections in this regime are a function of the elastic deformation of structural elements only, until the applied connection moment leads to gap opening. This resisting moment is provided by the clamping effect of the prestress within the beam-column interface. The column shear at gap opening is thus a function of the level of prestress provided by the beam tendons.

The column shear and displacements associated with gap-opening deflection can be calculated using beam bending theory and rigid body kinematics. The post gap-opening stiffness remains until the tendon elongation associated with the rigid body component reaches tendon yield. Further column deflection occurs with no further increase in column shear. Any inelastic tendon elongation reduces the post-tensioning force on unloading and subsequent cycles.

Modeling Initial Elastic Loading Behavior

Under initial elastic loading the beam and column deflect without gap-opening and contribute to total subassembly displacement. Figure 1 present a schematic diagram of the subassembly showing the associated nomenclature.

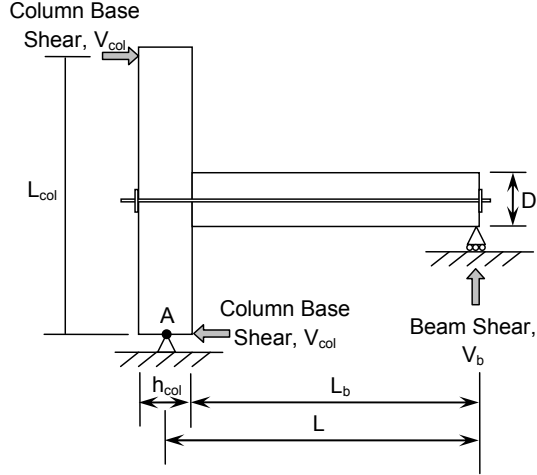


Figure 1. Beam-column subassembly nomenclature

During the initial elastic deformation regime the beam and column elastically deflects. The lateral deflection at the top of the column due to both beam and column deflection is defined as Δ_{col} and can be defined in relation to the applied column shear, V_{col} , as:

$$\Delta_{col} = V_{col} \left[\frac{(L_{col} - D)^3}{12EI_{col}^*} + \frac{L_{col}^2 L_b^2}{3LEI_b^*} \right] \quad (1)$$

where EI_{col}^* and EI_b^* are the effective column and beam stiffness values. The effective stiffness values have been approximated using moment area methods as 26% of the gross stiffness for uni-directional testing and 14% for bi-directional testing (Li et al. 2008).

Inclusion of Rigid Body Loading Behavior

Following the elastic deformation regime, the subassembly will undergo rigid-body rotation after gap-opening. This rigid body regime requires additions to the model for the post gap-opening regime and associated mechanics. The combination of pre gap-opening elastic beam deformation, post gap-opening deformation with elastic tendon elongation, and post gap-opening deformation with inelastic tendon elongation creates an overall tri-linear response. This overall loading path can be calculated based on elastic member deflection and rigid body rotation. Figure 2 presents the tri-linear elasto-plastic backbone curve for monotonic (pushover) behaviour of the subassembly. It includes the pre-gap-opening elastic deflection, and post-gap-opening behaviour, but does not include the effects of friction. Initial elastic deformation of the subassembly prior to gap-opening has stiffness (K_1+K_2) . Further elastic beam deflection and rigid body rotation after gap-opening gives stiffness K_2 . Finally, the unbonded post-tensioned tendons yield.

In Figure 2, M_{gap} is defined as the connection moment at gap opening. Here Δ_{gap} is the displacement at the top of the column from elastic deformation of the subassembly at gap opening. Further, Δ_{yield} is the displacement of the subassembly from beam deflection at the onset of plastic deformation of the post-tensioned tendons, which occurs at a connection moment of M_{yield} . All of the points shown in Figure 2 can be easily calculated from statics and kinematics, using the subassembly measurements in Figure 1.

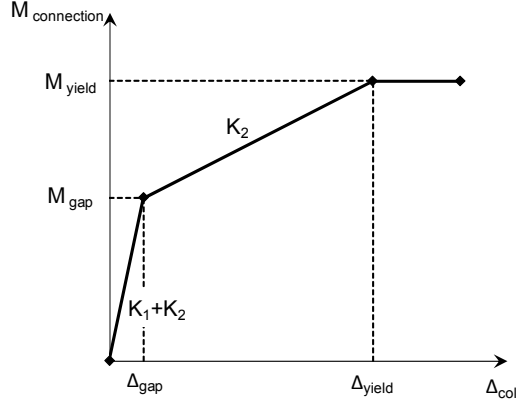


Figure 2. Bilinear-elastic-plastic monotonic backbone curve of a jointed precast system, where the connection moment is defined $M = V_{col}L_{col}$

The moment produced at the beam-column interface (rocking connection) at gap-opening, M_{gap} , under positive and negative rotations is respectively defined:

$$M_{gap} = F_{PT_initial} (j_{PT}^{\pm}) D \quad (2)$$

where $F_{PT_initial}$ is the total initial tensioning force in the tendons, j_{PT} is the fractional lever-arm of the tendon, the + and - indices refer to rocking about the bottom and top corners of the beam end, respectively, and D is the beam depth. Note that j^+ and j^- are proportional scalars of the beam depth with $j^+ + j^- = 1$. Note that due to the steel armored rocking interface, the beams rock essentially about their outer edge (the outermost fibre), so this model assumption is valid.

The displacement at the top of the column due to beam deflection at gap-opening, Δ_{gap} , is defined from the value of connection moment at gap-opening M_{gap} in Equation (2). Equation (1) can be re-written at gap opening using $V_{col,gap} = M_{gap}/L_{col}$:

$$\Delta_{gap} = \frac{M_{gap}}{L_{col}} \left[\frac{(L_{col} - D)^3}{12EI_{col}^*} + \frac{L_{col}^2 L_b^2}{3LEI_b^*} \right] \quad (3)$$

Moreover, the initial elastic stiffness of the subassembly, $(K_1 + K_2)$, as presented in Figure 2, can be calculated using Equations (2) and (3) and is defined:

$$K_1 + K_2 = \frac{L_{col}}{\left[\frac{(L_{col} - D)^3}{12EI_{col}^*} + \frac{L_{col}^2 L_b^2}{3LEI_b^*} \right]} \quad (4)$$

The connection moment and displacement at tendon yield can be similarly calculated, but occur at the point that plastic strain is induced in the tendons. This moment, M_{yield} , is given:

$$M_{yield} = \sigma_{yield} A_{PT} (j_{PT}^{\pm}) D = F_{PT_yield} (j_{PT}^{\pm}) D \quad (5)$$

where σ_{yield} is the yield stress of the tendons, A_{PT} is the total cross-sectional area of the tendons, and F_{PT_yield} is the total force in the tendons at yield.

Finally, the displacement at the top of the column at tendon yield, Δ_{yield} , can be defined as a sum of elastic and rigid body deflection components:

$$\Delta_{yield} = \frac{M_{yield}}{L_{col}} \left[\frac{(L_{col} - D)^3}{12EI_{col}^*} + \frac{L_{col}^2 L_b^2}{3LEI_b^*} \right] + L_{col} \frac{(\varepsilon_{yield} - \varepsilon_{initial})L_t}{\eta(j_{PT}^{\pm})D} \frac{L_b}{L} \quad (6)$$

where ε_{yield} is the total tendon strain at the onset of plastic deformation, $\varepsilon_{initial}$ is the initial strain in the tendons from post-tensioning alone before gap opening, L_t is the total length of the unbonded tendon, and η is the number of rocking interfaces spanned by the tendons.

Finally, the value of the post gap-opening stiffness, K_2 can easily be calculated from the geometry in Figure 2, and Equations (2), (3), (5), and (6). The stiffness is defined:

$$K_2 = \frac{(j_{PT}^{\pm})D(F_{PT,yield} - F_{PT,initial})}{L_{col} \frac{(\varepsilon_{yield} - \varepsilon_{initial})L_t}{\eta(j_{PT}^{\pm})D} \frac{L_b}{L} + \frac{(j_{PT}^{\pm})D(F_{PT,yield} - F_{PT,initial})}{L_{col}} \left[\frac{(L_{col} - D)^3}{12EI_{col}^*} + \frac{L_{col}^2 L_b^2}{3LEI_b^*} \right]} \quad (7)$$

The denominator can be segregated into a rigid body component (the first term) and post gap-opening elastic deflection component (the second term). If the elastic stiffness is much higher than the post gap-opening stiffness, then the rigid body component will have the major influence.

Incorporation of Prestress Friction Effects

If the connection utilizes a straight tendon profile and the duct is of a notably larger diameter than the tendon, it is unlikely any significant friction will exist. However, if a draped or bent tendon profile is utilized, as is commonly done for beams carrying gravity loads and for the seismic beams within this study, then frictional effects will affect cyclic loading performance.

Using the formula for prestress loss effects presented in Li et al. (2008) and assuming the product ($\mu_f \alpha_{PS}$) is small so that the higher order terms in the expanded exponential expression can be neglected, the prestress losses due to frictional effects, δF , is defined:

$$\delta F = F_{PT1} - F_{PT2} = \mu_f \alpha_{PS} F_{PT1} \quad (8)$$

where μ_f = angular coefficient of friction; α_{ps} = the angle change of the tendon (in radians); F_{PT2} = the prestress force at the joint face; and F_{PT1} = the applied jacking force to the prestress system. Note that this equation is an approximation of the force differential that exists within the tendon due to friction between the tendon and the duct it is located in.

Figure 3 presents the effect of friction on the monotonic pushover behaviour. The gap-opening resistance increases. Under cyclic loading, the stiffness changes due to frictional effects. By considering the mechanics of the connection, it is evident that friction within the tendon-duct system will affect the tendon force across the beam-column interface. A force differential will be present in the tendon where it contacts the duct. Upon reversal the tendon will relax before a force differential of an opposite sign exists. The elastic relaxation in the tendon during direction changes results in a stiffness, K_{fr} , shown in Figure 3, rather than a vertical force discontinuity, as predicted by using a signum function on the velocity to define to friction force (Li et al. 2008).

The elastic components are now defined as $(K_1 + K_2^+)$ for loading, and $(K_1 + K_2^-)$ for unloading, with the post-gap opening stiffness defined:

$$K_2^+ = K_{2_nom} (1 + \mu_f \alpha_{PS}) \quad (9a)$$

$$K_2^- = K_{2_nom} (1 - \mu_f \alpha_{PS}) \quad (9b)$$

where K_{2_nom} is the nominal post-gap opening stiffness, K_2 , without friction modification, defined in Equation (7), and shown in Figure 2. The intersection of the different K_2 lines, Δ_o , is the effective origin for the post-gap opening regime. With no initial post-tensioning, the initial elastic loading branch would not exist, and Δ_o would move to the axes origin, such that $\Delta_o = 0$.

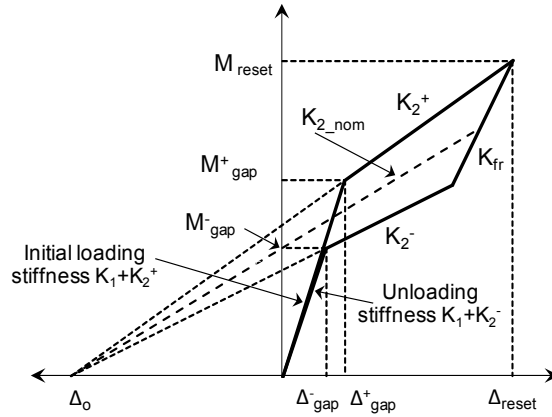


Figure 3. Schematic representation of the loading regime with the addition of friction. The dashed line labelled K_{2_nom} represents the post-gap opening stiffness without friction.

Loading Stiffness Definition

To computationally model this piece-wise linear behavior in a smooth continuous sense, differential versions of the Menegotto-Pinto(1973) and Ramberg-Osgood(1943) equations are used. To capture all of the different regimes in the response of Figure 3, it is necessary to develop different stiffnesses for the loading and unloading behaviour. The overall loading stiffness, $K^+(\Delta)$, has three different regions, as shown in Figure 3, and is defined:

$$K^+(\Delta) = K_1^{*+}(\Delta) + K_2^{*+}(\Delta) \quad (10)$$

where $K_1^{*+}(\Delta)$ is defined using a differential version of the Menegotto-Pinto equation:

$$K_1^{*+}(\Delta) = \frac{K_1}{\left\{ 1 + \left| \frac{M_{reset} + (K_1 + K_2^+)(\Delta - \Delta_{reset})}{K_1^+(\Delta - \Delta_o)} \right|^{R_p} \right\}^{(1/R_p+1)}} \quad (11)$$

where M_{reset} = the connection moment at the beginning of loading, and Δ_{reset} = the input displacement at the beginning of loading. The rate of change of the denominator at the transition

is defined by the value of R_p , with large values ($R_p \gg 10$), giving a very sharp transition, and lower values ($R_p \approx 2-5$), giving a more gradual transition and a more rounded response.

The stiffness component $K_2^{*+}(\Delta)$ should be active when the connection moment is less than that which corresponds to tendon yield and is defined:

$$K_2^{*+}(\Delta) = \frac{K_2^+}{1 + (R_y - 1) \left| \frac{M_{i-1}}{M_{yield}} \right|^{(R_y-1)}} \quad (12)$$

where R_y defines the rate of change of the gradient at the yield point, using a Ramberg-Osgood type formulation. Large values give a sharp transition and lower values a more gradual transition.

Unloading Stiffness Definition

To capture the different regimes in the unloading response it is necessary to develop a stiffness definition for the unloading behaviour similar to that used for loading. Similar to the loading path, the overall unloading stiffness, $K^-(\Delta)$, has three regions, as shown in Figure 3. The stiffness as a function of input displacement is defined as $K^-(\Delta)$. A line for the friction slope, K_{fr} , is defined relative to the reset point, similar to that utilised for loading in Equation (11).

From these observations, the unloading stiffness, $K^{*-}(\Delta)$, is defined:

$$K^-(\Delta) = K_1^{*-}(\Delta) + K_{fr} + K_2^{*-}(\Delta) \quad (13)$$

where K_{fr} is not dependent on response parameters, and $K_1^{*-}(\Delta)$ and $K_2^{*-}(\Delta)$ are defined:

$$K_1^{*-}(\Delta) = \frac{K_1}{\left\{ 1 + \left| \frac{K_1 \Delta}{-K_2^- \Delta_o} \right|^{R_p} \right\}^{(1/R_p+1)}} \quad (14)$$

$$K_2^{*-}(\Delta) = \frac{(K_2^- - K_{fr})}{\left\{ 1 + \left| \frac{\langle M_{reset} + K_{fr}(\Delta - \Delta_{reset}) \rangle}{K_2^-(\Delta - \Delta_o)} \right|^{R_{fr}} \right\}^{(1/R_{fr}+1)}} \quad (15)$$

where the McCauley's brackets term, indicated by $\langle \rangle$ is defined as $\langle A \rangle = A$ if $A > 0$, and $\langle A \rangle = 0$ if $A \leq 0$ for any value of input A . Thus, they are similar to the well-known Heaviside function. A detailed derivation of Equations (13)-(15) can be found in Rodgers(2009).

The initial connection moment at gap opening, M_{gap} can be calculated using Equation (2). From this value the origin of the K_2^+ and K_2^- lines, Δ_o (as defined in Figure 3) can be calculated from the geometry as:

$$\Delta_o = \frac{-K_1}{K_{2_nom}(K_1 + K_{2_nom})} M_{gap} \quad (16)$$

where K_2 = the nominal post gap-opening stiffness without modification for friction.

Although the model currently accounts for yielding within a response cycle due to the tri-linear behaviour, it must also account for the prestress force reduction on unloading and on subsequent cycles. Inelastic tendon elongation will result in a decrease in prestress force and alter the behavior on unloading and subsequent cycles. This reduction represents a shift in the location of the origin of the K_2^+ and K_2^- lines, Δ_o . The location of Δ_o changes by the amount of inelastic tendon elongation, and relocates to $\Delta_{o,new}$. The value of $\Delta_{o,new}$ is defined:

$$\Delta_{o,new} = \Delta_{reset} - \frac{M_{reset}}{K_2^+} \quad (17)$$

Equation (17) must only be implemented on a reset (when loading direction changes) and only when tendon yield has occurred (when $\Delta_{reset} > (\Delta_o + M_{yield} / K_2^+)$).

Overall Connection Modeling

The approach presented has been formulated as a subassembly model where the connection moment and displacement are always positive. The subassembly model can be considered to be formulated to give the connection moment for a normalized value of lever-arm, jD , where the fractional lever-arm, $j = 1.0$. The beam model will always yield positive moments, but the inclusion of the directionally dependent multiplier j corrects for the sign, providing the overall connection behaviour for both positive and negative connection displacements.

The connection moment at gap opening is linearly proportional to the magnitude of j . However, post-gap opening stiffness is proportional to the square of the fractional lever-arm, j . This relationship is explained by considering the underlying kinematics. Halving the magnitude of fractional lever-arm, j , will induce half the displacement in the tendon, and thus half the increase in tendon force. Furthermore, this force increase will only contribute half of the moment to the connection, due to the smaller lever arm, together providing the quadratic relationship. Figure 4 presents the schematic response for two values of j . The linear relationship for gap-opening connection moment, and quadratic relationship for post gap-opening stiffness results in the location of Δ_o being inversely proportional to magnitude of j .

Under cyclic loading the model must incorporate connection behaviour for positive and negative rotations with non-centrally located prestressing tendons ($j^+ \neq j^-$). Under these conditions, the model parameters, M_{gap} , M_{yield} , K_2 and Δ_o are all directionally dependent, as they are all a function of the fractional lever-arm, j , as defined in Equations (2), (5), (7), and (15), respectively. To accommodate this directional dependence, the values need to be switched based on the direction of loading, and the associated value of either j_{PT}^+ or j_{PT}^- . However, all other model equations hold given this switching to account for the directional response behavior.

This switching can be implemented a number of ways, including: 1) using conditional statements, or 2) incorporating a switching function using Heaviside, sigmoid or hyperbolic tangents functions. The implementation is straightforward computationally and only requires that the values be assigned at any change in sign of the input displacement. The directional dependence of Δ_o can be incorporated into the model using Equations (2) and (16).

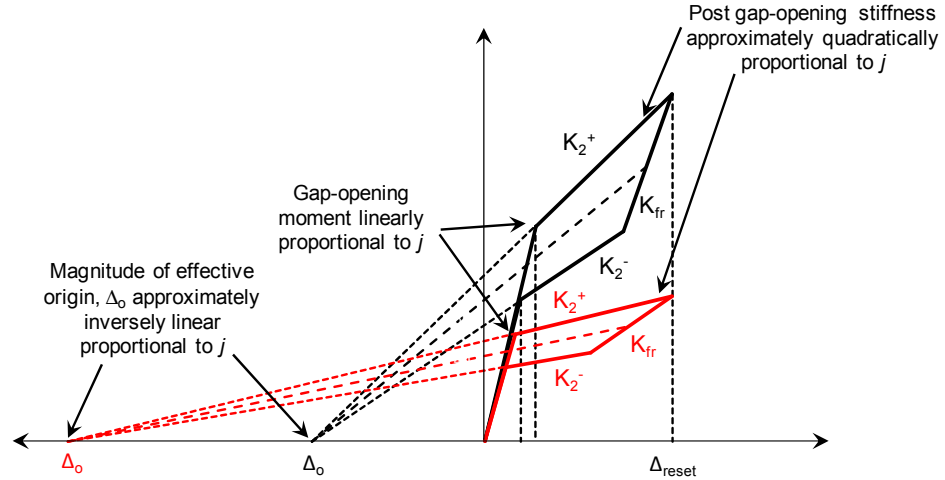


Figure 4. Representation of the dependence of Δ_0 on the fractional lever-arm, j .

Model Implementation

The overall tangent stiffness is defined as K_t , and incorporates the model developed in the previous sections, accounting for elastic flexibility and contributions from rigid body rotations and tendon behaviour, defined in Equations (10) to (15). This model includes the modifications presented to account for friction, yielding, prestress reduction, and overall connection behaviour/directional dependence. The tangent stiffness can be used in a time-incremental formulation to relate column displacement, Δ , to connection moment or column shear.

Experimental Validation

The experimental corner joint configuration presented in Li et al. (2008) and Rodgers (2009) utilising a bent tendon profile was chosen for experimental validation. This configuration presents very complex overall hysteretic response that captures almost all of the considerations presented in the model development. The experimental specimen had basic dimensions, defined in Figure 1, of $L_{col} = 2.9\text{m}$, $h_{col} = 0.7\text{m}$, $L = 4\text{m}$, $L_b = 3.65\text{m}$, and $D = 0.56\text{m}$. In the experiment, for positive joint rotations, $j_{PT}^+ = 0.66$, and $D = 560\text{mm}$ so that $(jD)_{PT}^+ = 370\text{mm}$, and for negative joint rotations, $j_{PT}^- = 0.34$ so that $(jD)_{PT}^- = 190\text{mm}$.

Results and Discussion

The test specimen underwent quasi-static uni-directional displacement tests in the seismic direction using fully reversed sine wave profiles up to 4% inter-storey drift. The experimental data for the exterior connection was utilized as it is the most difficult case to model due to the asymmetry in gap opening force, friction, and yield displacement. Therefore, the exterior connection is the most stringent test of the model, and once validated can be extended to also model the symmetrical joints if desired. Figure 5 presents the experimental and model results for the subassembly. Overall, very good agreement is evident between the computational model and the experimental results. The subassembly shows very good agreement, and captures the tendon yield, friction, and loss of prestress following large response cycles causing tendon yield.

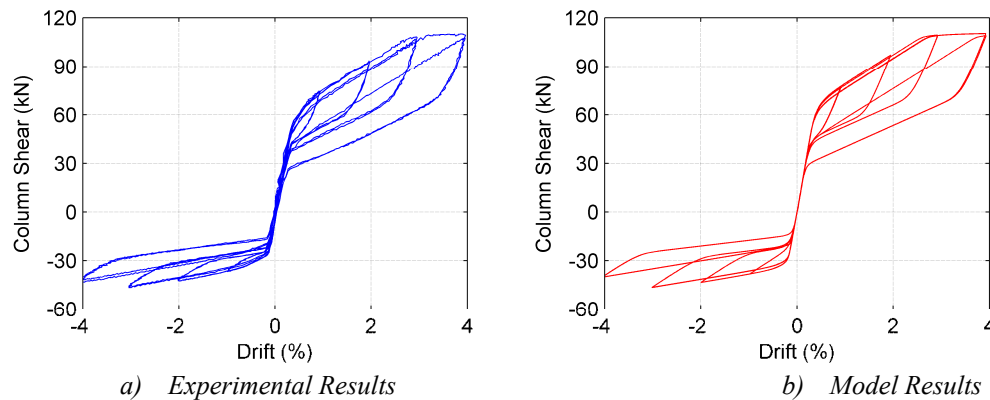


Figure 5. Comparative results

Conclusion

The advanced model of joint hysteresis using time-incremental differential functions of the Menegotto-Pinto and Ramberg-Osgood type show very good agreement with the experimental results. The ability to accurately predict the entire hysteretic response at any drift level is an important outcome for analysis purposes. Overall, this model is more complex than simpler explicit forms in previous research, but provides a much more robust description. If significant friction or tendon yield is present then the simpler explicit models will not provide accurate results. Friction, yielding and prestress reduction are all modeled explicitly; it is considered that this leads to the good overall agreement with the experimental observations.

Acknowledgements

This work was developed while the first author was at Texas A&M University on a Fulbright-EQC Graduate Award. The support of Fulbright New Zealand, the New Zealand Earthquake Commission, and the New Zealand Tertiary Education Commission is gratefully acknowledged.

References

- Li, L., Mander, J. B., and Dhakal, R. P. (2008). "Bi-Directional Cyclic Loading Experiment on a 3-D Beam-Column Joint Designed for Damage Avoidance." *J. of Struct Engr*, 134(11), 1733-1742.
- Mander, J. B. (2004). "Beyond ductility: The quest goes on." *Bulletin of the New Zealand Society for Earthquake Engineering*, 37(1), 35-44.
- Menegotto, M., and Pinto, P. (1973). "Method of analysis for cyclically loaded reinforced concrete plane frames including changes in geometry and non-elastic behavior of elements under combined normal force and bending." *IABSE Symposium on the Resistance and Ultimate Deformability of Structures Acted on by Well-defined Repeated Loads*, Lisbon.
- Priestley, M. J. N., Sritharan, S., Conley, J. R., and Pampanin, S. (1999). "Preliminary results and conclusions from the PRESSS five-story precast concrete test building." *PCI Journal*, 44(6), 42-67.
- Ramberg, W., and Osgood, W. R. (1943). "Description of Stress-strain Curves by Three Parameters." *National Advisory Committee on Aeronautics, Technical Note 902*.
- Rodgers, G. W. (2009). "Next Generation Structural Technologies: Implementing High Force-To-Volume Energy Absorbers," *PhD Thesis*, University of Canterbury, Christchurch, New Zealand.
- Rodgers, G. W., Solberg, K. M., Mander, J. B., Chase, J. G., Bradley, B. A., Dhakal, R. P., and Li, L. (2008). "Performance Of A Damage-Protected Beam-Column Subassembly Utilizing External HF2V Energy Dissipation Devices." *Earthquake Engineering & Structural Dynamics*, 37(13), 1549-1564.
- Solberg, K. M. (2007). "Experimental and financial investigations into the further development of damage avoidance design," *Master of Engineering Thesis*, Univ. of Canterbury, Christchurch, NZ.